RSC Advances

PAPER

View Article Online
View Journal | View Issue

Cite this: *RSC Adv.*, 2023, **13**, 15311

Functionalization of cellulose nanocrystals extracted from pineapple leaves as a UV-absorbing agent in poly(lactic acid)

Kanokporn Pornbencha,[ab] Sarannuch Sringam,[ab] Supicha Piyanirund,[ab] Anusorn Seubsai,[ab] Paweena Prapainainar,[ab] Chalida Niumnuy,[ab] Supacharee Roddecha[ab] and Peerapan Dittanet *[ab]

The cinnamate functionalization of cellulose nanocrystals (Cin-CNCs) was investigated as a potential organic reinforcing and UV-shielding agent in polylactic acid (PLA) films. Acid hydrolysis was used to extract cellulose nanocrystals (CNCs) from pineapple leaves. Through esterification with cinnamoyl chloride, the cinnamate group was grafted onto the CNC surface and the resulting Cin-CNCs were incorporated in PLA films as reinforcing and UV-shielding agents. The PLA nanocomposite films were prepared using a solution-casting method and were tested for mechanical/thermal properties, gas permeability, and UV absorption. Importantly, the functionalization of cinnamate on CNCs substantially improved the dispersion of fillers on the PLA matrix. The PLA films containing 3 wt% Cin-CNCs exhibited high transparency and UV absorption in the visible region. On the other hand, PLA films filled with pristine CNCs did not exhibit any UV-shielding properties. The mechanical properties revealed that adding 3 wt% Cin-CNCs to PLA increased its tensile strength and Young's modulus by 70% and 37%, respectively, compared to neat PLA. In addition, the incorporation of Cin-CNCs substantially improved water vapor and oxygen permeability. At 3 wt% Cin-CNC addition, the water vapor and oxygen permeability of PLA films were reduced by 54% and 55%, respectively. This study demonstrated the great potential in utilizing Cin-CNCs as effective gas barriers, dispersible nanoparticles, and UV-absorbing, nano-reinforcing agents in PLA films.

Received 23rd April 2023
Accepted 15th May 2023

DOI: 10.1039/d3ra02693k

rsc.li/rsc-advances

1. Introduction

Polylactic acid (PLA) is one of the most widely used biodegradable plastics as a substitute for petroleum-based plastics. PLA is made of lactic acid, containing a monomer from the fermentation of dextrose by bacteria or renewable sources.[1,2] PLA has the advantages of good transparency, environmental friendliness, and biological compatibility. However, PLA has some drawbacks, such as hydrophobicity, low strength, brittleness, and poor thermal stability, which cause manufacturing challenges.[2–4] Cellulose nanocrystals (CNCs) have been a focus of attention as one of the most effective modifiers to improve the properties of PLA. The addition of functional CNCs to PLA provides high mechanical strength, good thermal stability, low water/gas permeability, and good optical properties.[5,6] Furthermore, when PLA is exposed to heat and ultraviolet (UV) light, its gradual degradation can cause discoloration and microcracking, limiting its use in outdoor applications and reducing the lifetime of PLA-based products. In these applications, the use of thermal and UV absorbers can be applied. However, many commercial UV absorbers contain heavy metals, such as lead or titanium dioxide (TiO_2) which can be harmful to the environment. Recently, sustainable bio-sourced materials, such as cinnamates, have been reported as effective UV absorbers due to their strong absorption band in the UV range, typically between 280 and 340 nm. This allows them to absorb the UV radiation and convert it into heat, which is dissipated harmlessly into the surrounding environment. In addition, cinnamates are highly effective at low concentrations, typically 0.1–1% of cinnamate. They are non-toxic and environment-friendly, making them an attractive option for applications where safety and sustainability are important. Furthermore, they are compatible with a wide range of polymers and can be incorporated easily into polymer formulations without affecting the processing or mechanical properties. In this work, we developed cinnamate-functionalized CNCs for use in PLA film as reinforcing and UV-shielding agents.

CNCs are produced by breaking down cellulose fibers through chemical or mechanical methods. Cellulose is one of the most abundant materials in nature and can be obtained from bio-wastes, such as cotton stalks, fruit residues, and forest

[a]*Department of Chemical Engineering, Faculty of Engineering, Kasetsart University, Bangkok 10900, Thailand. E-mail: peerapan.d@ku.th*
[b]*Center of Excellence on Petrochemical and Materials Technology, Kasetsart University, Bangkok 10900, Thailand*

residues.[7,8] Pineapple leaves are a byproduct of the fruit industry that is generated on a regular basis and is often discarded, particularly in Thailand. Pineapple leaves are a rich source of cellulose, as a result, the production of cellulose-based materials allows for waste reduction and the creation of value-added products. Moreover, pineapple leaf fibers are particularly well-suited for the manufacturing of cellulose-based products because they are long and reasonably straight, making extraction and processing simple.[9] Cellulose is a polysaccharide made up of a linear chain of β-(1–4)-glycosidic linkages.[10] These regular arrangements of the OH-group along the surface of cellulose produce crystalline properties. The extraction of CNCs from natural wastes had been extensively studied. For example, Alothman *et al.*[11] extracted CNCs from date palm fiber by hydrolyzing it using a mixture of sulfuric acid and acetic acid. The CNCs were rod-shaped and used as a reinforcing agent in a variety of industrial areas. Zhang *et al.*[12] extracted CNCs from lemon seeds and compared two different extraction techniques. Sulfuric acid hydrolysis produced CNCs that were about 12–25 nm in diameter and 130–170 nm in length, with the highest crystallinity; however, a low yield was reported. Fortunati *et al.*[13] successfully extracted CNCs from *Posidonia oceanica* plant waste through hydrolysis using sulfuric acid and incorporated them with PLA to improve their properties. CNCs have many advantages, including being rich in cellulose, fully biodegradable and renewable, and having high strength, high modulus, and good flexibility. However, the hydrophilic nature of CNCs can limit their compatibility with the hydrophobic nature of a polymer matrix, leading to a decrease in mechanical properties.[14] A common way to increase dispersibility in a polymer matrix is to modify the hydroxyl groups through covalent functionalization with a range of esters, carboxylic acids, ethers, or silane coupling agents.[5,6]

Cinnamates are found in numerous plants and fruits, including cinnamon, strawberries, and eucalypts.[15,16] Cinnamates had been used as grafting agents in polymers. For example, Wang *et al.*[17] studied cinnamate-functionalized natural carbohydrates (Cin-Carb) as thin-film transistors. Wu *et al.*[18] prepared UV-curable films using cinnamate-functionalized rubber where functionalization was achieved by reacting cinnamoyl chloride with hydroxyl-functionalized butyl rubber. Zhu *et al.*[19] prepared biodegradable elastomers used in soft medical devices based on cinnamate-functionalized polyesters. Bugatti *et al.*[20] developed nano-hybrids consisting of a layered double hydroxide with a cinnamate anion for green pesticides, which were compatible with a pectin matrix for green protective coatings for crop protection. The functionalization of the cinnamate group on the CNC surface has shown promise in improving dispersion ability in a polymer matrix.[15] In addition, cinnamate-functionalized-CNCs can enhance UV-shielding properties, making them a suitable material for various applications in the packaging, automotive, and biomedical industries. The chemical structure of cinnamate contains a chromophore comprised of conjugated benzene rings and neighboring carbon double bonds. This conjugated structure enables the cinnamate to have high absorption for UV radiation. Cinnamate groups can be grafted on the nanocellulose surface through an acylation reaction with an excess of cinnamoyl chloride.[16] The present study focuses on green environmental, renewable, and sustainable resources. The most popular UV-shielded materials in thin film polymer are metal oxide nanoparticles such as SiO_2, ZnO or TiO_2;[21,22] however, they contain heavy metals, have low transparency and are not environment-friendly. Hence, functionalization of the cinnamate group onto CNCs could be alternative approach for green industry.

In this paper, we investigated the use of cinnamate-based cellulose nanocrystals (Cin-CNCs) as potential nanofillers in PLA films for UV-shielding applications. Acid hydrolysis was used to extract CNCs from pineapple leaves. Cin-CNCs were prepared by grafting the cinnamate group onto the surface of CNCs using an esterification reaction. PLA/Cin-CNC films were prepared by a simple solution-casting method. The properties of Cin-CNCs were characterized by Fourier transform infrared (FTIR) spectrometer, X-ray diffraction (XRD), scanning electron microscope (SEM), transmission electron microscope (TEM), and thermal gravimetry analysis (TGA). The effects of functionalization on the properties of the PLA nanocomposite films were characterized for their thermal, mechanical, optical, permeability, and UV-absorption properties.

2. Experimental

2.1 Materials

Dried pineapple leaves were received from southern Thailand. Sodium hydroxide (NaOH), sodium chlorite ($NaClO_2$), glacial acetic acid (CH_3COOH), sulfuric acid (H_2SO_4), dimethylformamide (DMF), dimethylaminopyridine (DMAP), triethylamide (TEA), and cinnamoyl chloride, chloroform ($CHCl_3$) received from Labsystems (Thailand) Co., Ltd. Poly(lactic acid) (PLA) (3052D, $M_w = 116\,000$ g mol^{-1}, density = 1.24 g cm^{-3}) in pellet form was purchased from Nature Works Asia Pacific, Thailand.

2.2 Nanocellulose extraction

Pineapple leaves (PAL) were washed, dried, and ground into powder using a blender. The dried PAL powder was passed through a 250-mesh sieves before use. To remove lignin and hemicellulose, 1 g of PAL were treated by 20 mL of 4% NaOH at 100 °C for 2 hours, then filtered and rinsed with distilled water until the pH was neutral. After alkaline treatment, the filtered residue was dried to produce a brownish powder of pineapple leaves (APAL). Then, the APAL was bleached in a solution consisting of 6 g of $NaClO_2$, 2 mL of CH_3COOH, and 640 mL of DI water. The APAL powder was stirred in the bleaching solution at 60 °C for 1 hour, then filtered, washed, dried, and milled into powder. This procedure was repeated three times or until the color of the APAL power had changed to white. After chemical treatment, the powder of pineapple leaves after bleaching (BPAL) was hydrolyzed with 64% H_2SO_4 at 60 °C for 1 hour. Excess cold DI water was added to stop the reaction; the mixture was centrifuged at 7500 rpm for 15 minutes to remove excess acid and small particles. The suspension was dialyzed with DI water until the pH was neutral to obtain CNCs. The CNCs were

sonicated for 30 minutes and kept in refrigerator at 4 °C before use.

2.3 Functionalization of nanocellulose by cinnamate group (Cin-CNCs)

Samples (1 g) of CNCs were sonicated for 5 minutes in 80 mL of DMF. Then, the solution was ultrasonically mixed with 2.58 mL of TEA and 1.13 g of DMAP for 5 minutes. An ice bath was used to cool the mixed solution to 0 °C. After dissolving 3.3 g of cinnamoyl chloride in 20 mL of DMF, the solution was added to the cooled, mixed solution. The reaction was carried out at room temperature for 24 hours. Dialysis with DI water was used to remove the solvent. Finally, the cinnamate-modified cellulose (Cin-CNCs) powder was obtained by freeze-drying the suspension.

2.4 Preparation of PLA nanocomposite films

The PLA was dried at 40 °C for 24 hours to remove moisture. At 60 °C, 1 g of PLA was dissolved in 30 mL of $CHCl_3$. CNC or Cin-CNC powders (0, 0.5, 1.0, 3.0, or 5.0 wt%) were dispersed in 10 mL of $CHCl_3$ and sonicated for 5 minutes before adding to the PLA solution. At 60 °C, each mixed solution was stirred for 10 minutes, before sonicating for 5 minutes and stirring in a water bath at 60 °C for 5 minutes. Finally, the mixture solution was poured into a cleaned glass mold (16.5 cm × 16.5 cm) and dried for 12 hours at 45 °C. The resultant PLA nanocomposite films were designated PLA/CNC-x% and PLA/Cin-CNC-x% where x was the percentage by weight (wt%) of CNCs or Cin-CNCs.

2.5 Characterizations

(1) The chemical compositions of PAL, APAL, and BPAL were investigated using TAPPI standard methods.[23]

(2) The chemical structures of sample materials were measured in the range 400–4000 cm^{-1} using Fourier transform infrared (FT-IR) spectroscopy (PerkinElmer Spectrum 100) at a resolution of 2 cm^{-1}.

(3) The surface morphologies of the samples were examined at an accelerating voltage of 15 kV using SEM (FEI Quanta 450). Samples were coated with gold before examination.

(4) X-ray diffraction (XRD) patterns of the CNCs and Cin-CNCs were studied using an XRD diffractometer (Philips X′ Pert) with 2θ angle ranges from 5° to 45°. The test was performed at a scan rate of 2 min^{-1}. Eqn (1) was used to calculate the crystallinity index (C_I) of nanocellulose:

$$C_I = \frac{I_{(002)} - I_{am}}{I_{(002)}} \quad (1)$$

where $I_{(002)}$ is the maximum intensity of lattice diffraction at $2\theta = 22°$ and I_{am} is the diffraction intensity of an amorphous region of nanocellulose at $2\theta = 15°$.[24]

(5) The morphologies of the CNCs and Cin-CNCs were studied using transmission electron microscopy (TEM; Hitachi, HT7700) at an accelerating voltage of 80 kV. The samples were diluted 200 times with DI water. Before investigation, the suspensions were placed on a 200-mesh copper grid, colored with 2% uranyl acetate for 10 minutes, and dried at room temperature for 1–2 days.

(6) Thermogravimetric analysis (Mettler Toledo, TGA2) was used to examine the thermal stabilities of the CNC and Cin-CNC nanoparticles at temperatures in the range 30–600 °C, with a flow rate of 50 mL min^{-1} and a heating rate of 10 °C min^{-1}.

(7) Differential scanning calorimetry (PerkinElmer, DSC 8000) was used to investigate the crystallization behavior of the PLA nanocomposite films at temperatures in the range 30–200 °C. All samples were evaluated at a heating rate of 10 °C min^{-1}, in a nitrogen atmosphere at a flow rate of 50 mL min^{-1}. To eliminate the history of sample preparation, the DSC result of the second heating was reported.

(8) The mechanical properties of the PLA nanocomposite films were studied using a universal test machine (UTM; Instron, 5965) in accordance with the ASTM D882 standard method.[25] The samples were cut into 25 × 100 mm pieces and the speed test was 5 mm min^{-1}. At least five samples were reported for each formulation.

(9) The water vapor transmission rate (WVTR) of the PLA nanocomposite films was investigated using a Mocon: PERMATRAN-W®398 instrument in accordance with the ASTM E398-03 standard method at 37.8 °C and 90% humidity.[26] The water vapor permeability (WVP) was calculated using eqn (2):

$$WVP = \left[\frac{WVTR}{P_{sat}(RH_{out} - RH_{in})}\right] \times L \quad (2)$$

where P_{sat} is the saturated pressure of water vapor at 37.8 °C (kPa), RH_{out} is the relative humidity of the external sides of the film (test RH), RH_{in} is the relative humidity of the internal sides of the film (~0%), and L is the film thickness.[27]

(10) The oxygen transmission rate (OTR) of the PLA nanocomposite films were investigated using an OTR 8101 Illinois instrument, following the ASTM D-3985 standard method at 25 °C.[28] The oxygen permeability (OP) was calculated using eqn (3):

$$OP = \frac{OTR \times L}{\Delta P} \quad (3)$$

where L is the film thickness and ΔP is the difference in partial pressure of the permeant (O_2) across the sample (101 325 Pa).[27]

(11) The UV radiation absorption of the PLA nanocomposite films was tested in the wavelength 200–400 nm using a UV-Vis-NIR spectrophotometer equipped with a universal measurement accessory (PerkinElmer LAMBDA 1050). The films were cut into 3 × 3 cm squares prior to examination.

3. Results and discussion

3.1 Characterization of CNCs and Cin-CNCs extracted from pineapple leaves

The physical appearances of the pineapple leaves (PAL), pineapple leaves after alkali treatment (APAL), and pineapple leaves after bleaching (BPAL) are shown in Fig. 1a–c. The color of the PAL powder changed from yellowish-brown to white after chemical treatment due to the removal of lignin. The chemical

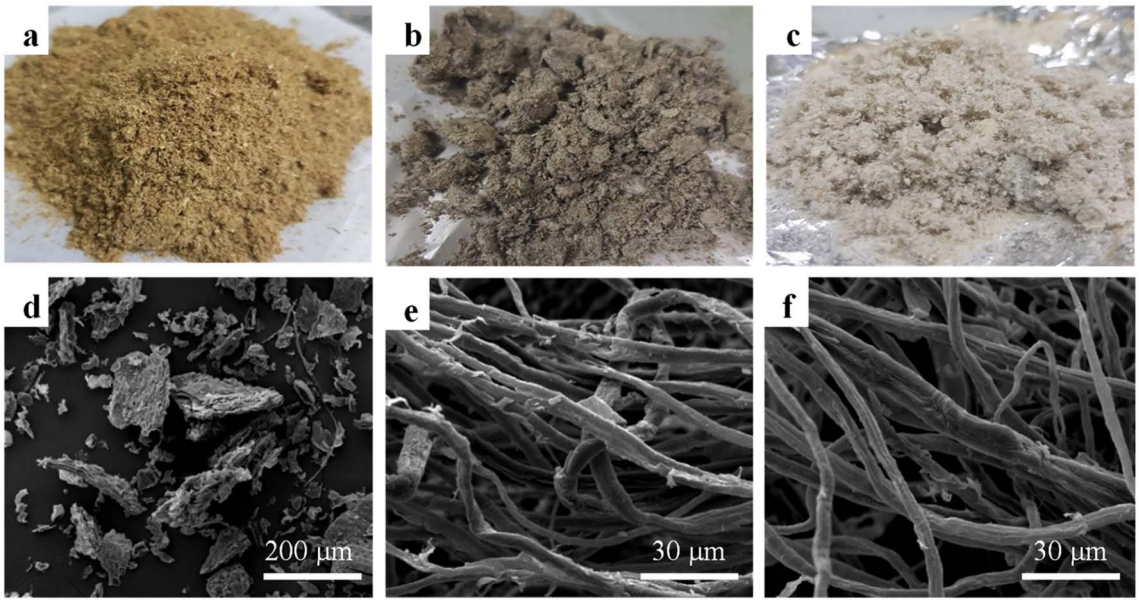

Fig. 1 Morphological structures of (a and d) the pineapple leaves (PAL), (b and e) pineapple leaves after alkali treatment (APAL), and (c and f) pineapple leaves after bleaching (BPAL).

Table 1 Chemical compositions of PAL, APAL, and BPAL

	Chemical component (%)			
Sample	Cellulose	Hemicellulose	Lignin	Extractives[a]
PAL	20.61 ± 0.62	22.19 ± 0.23	25.62 ± 1.48	31.58 ± 2.18
APAL	30.17 ± 0.73	20.63 ± 0.91	14.88 ± 0.14	34.32 ± 1.29
BPAL	50.00 ± 0.79	17.60 ± 0.45	7.44 ± 0.59	24.96 ± 1.03

[a] Extractives included fat, wax, oil, tanning, and pectin in ethanol + benzene, ethanol, and hot water.[29] The standard deviation was calculated using three measurements.

compositions of PAL measured before and after chemical treatment based on the TAPPI standard methods are shown in Table 1. As expected, the cellulose content increased after chemical treatment from 20.61 ± 0.62% (PAL) to 50.00 ± 0.79% (APAL). Consequently, the lignin and hemicellulose in PAL substantially decreased after chemical treatment from 25.62 ± 1.48% (PAL) to 7.44 ± 0.59% (BPAL) and from 22.19 ± 0.23% (PAL) to 17.60 ± 0.45% (BPAL), respectively.

The SEM characterizations of the PAL, APAL, and BPAL are shown in Fig. 1d–f. PAL contained irregular shape particles with a relatively rough surface, as shown in Fig. 1d. On the other hand, APAL and BPAL exhibited a long, fiber-like structure with average diameters of approximately 7–10 μm. The surface of the APAL and BPAL fibers were comparatively smooth compared to the surface of the PAL, indicating that impurities, lignin, and unsaturated molecules had been removed by the chemical treatment. Fig. 2a shows the TEM characterization of the CNCs, with a rod-like morphology. After the esterification reaction, the

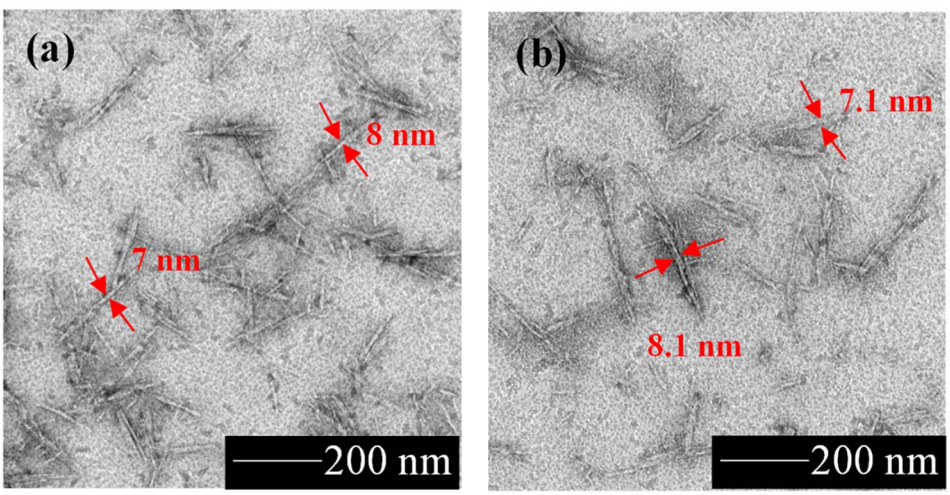

Fig. 2 Morphological structure of (a) CNCs and (b) Cin-CNCs, where red arrows indicate diameters of nanoparticles.

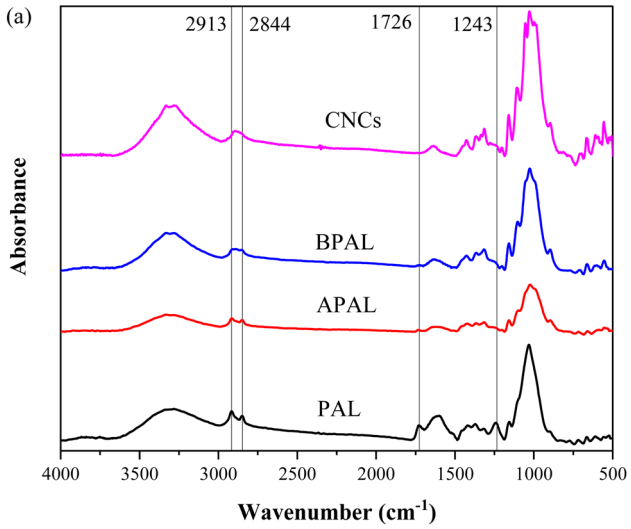

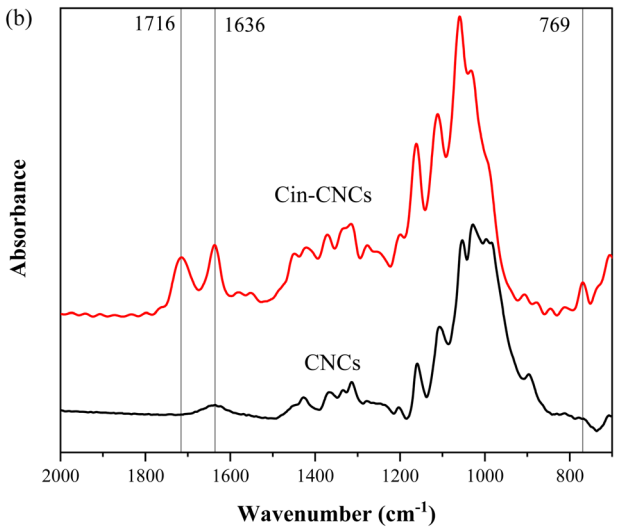

Fig. 3 FTIR spectra of (a) PAL, APAL, BPAL, and CNCs, and (b) CNCs and Cin-CNCs.

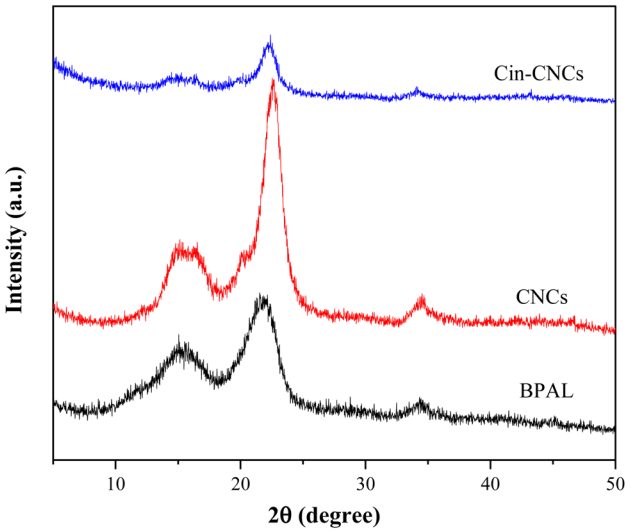

Fig. 4 XRD patterns of BPAL, CNCs, and Cin-CNCs.

Cin-CNCs retained the rod-like structure of the cellulose nanocrystals with an average diameter and length of 7 ± 2.04 nm and 98 ± 16.59 nm, respectively.

The FTIR spectra of the PAL, APAL, BPAL and CNCs are shown in Fig. 3a. All spectra exhibited broad peaks from 3000 cm^{-1} to 3500 cm^{-1} of O–H stretching[29] and sharp peaks at 2913 cm^{-1} and 2844 cm^{-1} from C–H stretching of cellulose molecules.[24] For PAL and APAL, the hydroxyl groups were bound by lignin, waxes and hemicelluloses; therefore, the intensities of these peaks were boarder compared to those of BPAL and CNCs. All samples exhibited the characteristic peaks of 1243 cm^{-1} and 1726 cm^{-1}, which can be ascribed to C–O stretching of lignin and hemicellulose molecules, and C=O stretching of α, β-unsaturated ester molecules of lignin, respectively.[30] These peaks decreased after chemical treatment using NaOH and $NaClO_2$ and completely disappeared after the acid hydrolysis treatment to obtain CNCs. As shown in the FTIR spectra of CNC, the absence of 1243 cm^{-1} and 1726 cm^{-1} peaks indicated the complete removal of lignin and hemicelluloses.

The FTIR spectra of the CNCs and Cin-CNCs are shown in Fig. 3b. Cin-CNCs spectra exhibited peaks at 769 cm^{-1}, 1636 cm^{-1}, and 1716 cm^{-1} corresponding to out-of-plane aromatic C–H bending, C=O stretching, and C=C stretching, respectively.[17] This result confirmed the reaction of surface hydroxyl groups with cinnamoyl chloride and an acylating agent, inidcating that grafting the cinnamate group onto the surface of CNCs was successful.

Fig. 4 shows the XRD patterns of the BPAL, CNCs and Cin-CNCs. All the samples exhibited peaks at $2\theta = 15°$ (plane 101), 22° (plane 002), and 35° (plane 004) indicating cellulose type I,[31,32] which is normally found in plants and following biosynthesis from bacteria. The calculated crystallinity index values of the BPAL, CNCs, and Cin-CNCs were 25.82%, 60.34%, and 51.94%, respectively. The progressive removal of the amorphous structure in the CNCs due to acid hydrolysis caused an increase in the crystallinity index from the BPAL to the CNCs. Conversely, the crystallinity index of Cin-CNCs decreased due to substitution of the OH group by the cinnamate.[33] Since the molecular structure of the cinnamate was much larger than for the OH group, there was a greater distance between polymer chains, resulting in the structure becoming more amorphous, with a resultant decrease in crystallinity.

The thermal stability of the CNCs and Cin-CNCs was measured using TGA. Fig. 5 depicts the percent and derivative weight loss as a function of temperature. The small weight loss in the temperature range 30–100 °C was due to the removal of moisture in samples. It was clear that the Cin-CNC particles had a smaller weight loss and less moisture absorbed compared to the CNC particles due to hydrophobic surface structure of the cinnamate group. The decomposition temperature of the CNCs was in the ranged 220–360 °C with T_d at 267.2 °C, which was consistent with literature data.[30] A two-step decomposition

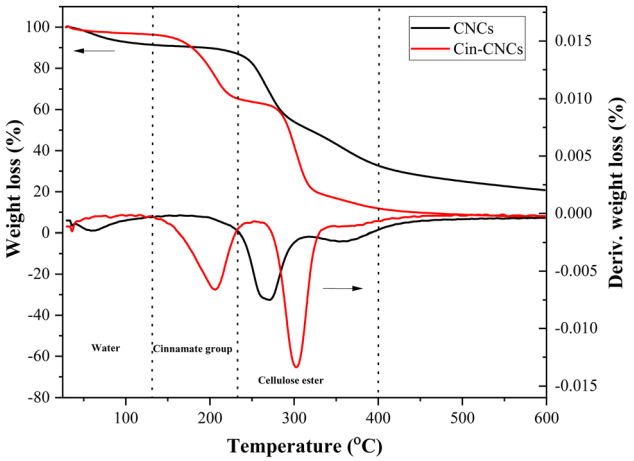

Fig. 5 TGA thermograms curves of CNCs and Cin-CNCs.

behavior was observed in the Cin-CNCs. The cleavage of the cinnamate group was associated with the first weight loss at a low degradation temperature (207.6 °C).[16] The higher degradation temperature (300.5 °C) corresponded to cellulose ester.[34] This result indicated that the grafting of cinnamate group onto CNCs was successful.

3.2 Properties of PLA nanocomposite films

3.2.1 Physical appearance. Fig. 6 shows pure PLA film and PLA nanocomposite film prepared by solvent-casting technique. Pure PLA film was homogenous and had a highly transparent surface, while the PLA/CNC films were homogenous and had a transparent characteristic only at low CNC content (up to 1 wt%). At higher contents of CNCs, the nanocomposite films had a rough surface and was slightly opaque due to agglomerations of CNCs. However, the film was still macroscopically transparent. For the PLA/Cin-CNC films, no aggregation of Cin-CNCs in PLA matrices was observed in any of the formulations. The PLA/Cin-CNC films were homogeneous and highly transparent, indicating good miscibility between the Cin-CNCs and PLA.

3.2.2 Glass transition temperature (T_g) and melting temperature (T_m). Fig. 7 depicts the DSC thermograms of the pure PLA, PLA/CNC, and PLA/Cin-CNC nanocomposite films. All samples exhibited glass transition, cold crystallization, and melting transition. The T_g value of the pure PLA was 58 °C, which was consistent with the T_g of PLA prepared using solvent casting,[4] as shown in Table 2. No significant change in T_g was observed with the addition of CNCs up to 3 wt%. However, the T_g value decreased to 55 °C at 5 wt% of CNC content. With the addition of Cin-CNCs, the T_g value was slightly lower at 57 °C for a low Cin-CNC content and continued to decrease with increasing filler content. A decrease in the T_g in the PLA/Cin-CNCs was attributed to an increase in the molecular motion of the polymer chain after grafting the cinnamate group onto the Cin-CNC surfaces. This branching chain of the cinnamate group resulted in a steric structure, generating more free volume that resulted in a lower T_g.[35–37]

In addition, the presence of CNCs and Cin-CNCs affected the cold crystallization temperature (T_{cc}) and the melting temperature (T_m) of the PLA. The cold crystallization peak resulted from the incomplete crystallization of the samples during film casting. The T_{cc} value of pure PLA was 116 °C; however, with the addition of CNCs, this decreased slightly to 110–113 °C. Furthermore, with the addition of Cin-CNCs, the T_{cc} value decreased substantially 104–108 °C as a result of the enhanced chain mobility.[35] The pure PLA exhibited only one sharp peak of the T_m at 149 °C,[36] while the PLA/CNC and PLA/Cin-CNC films had double melting peaks for all formulations. At a low content of CNCs, the PLA/CNC films had a sharp peak with a small shoulder; however, at higher CNC contents, a bimodal melting peak was more pronounced. The T_{m1} and T_{m2} values of the PLA/CNC films were in the ranges 141–148 °C and 150–153 °C, respectively. In the PLA/Cin-CNC films, bimodal melting peaks were clearly seen at low filler contents. The T_{m1} and T_{m2} values

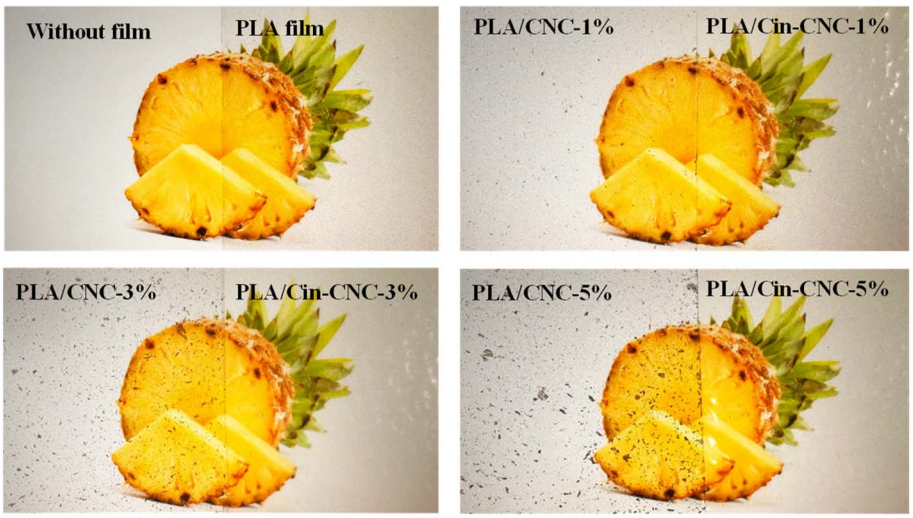

Fig. 6 Physical characteristics of pure PLA and PLA nanocomposite films.

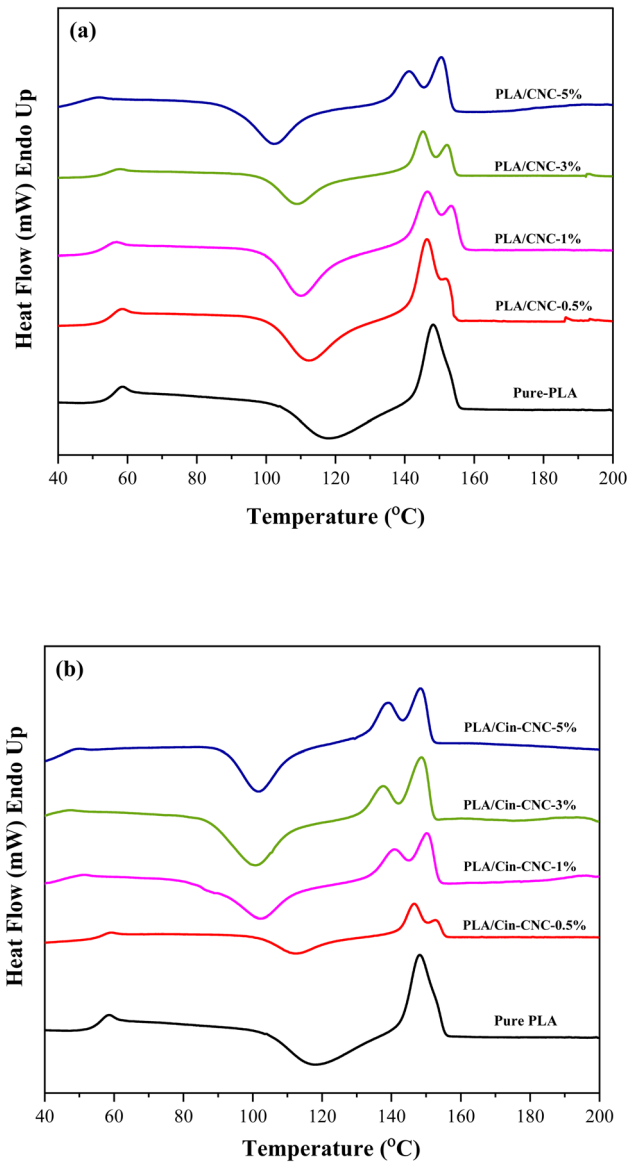

Fig. 7 DSC curves of (a) PLA/CNC films and (b) PLA/Cin-CNC films.

of the PLA/Cin-CNCs were in the ranges 138–146 °C and 148–152 °C, respectively.

These bimodal melting peaks, which appeared in all the PLA nanocomposites, are usually caused by melting due to a dual morphological mechanism, reported by other researchers.[35–37] PLA is a semi-crystalline thermoplastic polymer. Based on the lamellar thickness model,[37] this double endothermic behavior results from the existence of two different kinds of crystal lamellae and thicknesses in the structure. Thinner flakes will start to melt fist in association with a lower endothermic temperature (T_{m1}). The melting of thicker lamellae occurs at a higher temperature endotherm (T_{m2}). When cellulose nanocrystals are introduced into polymer matrix, they can act as impurities or nucleating agents that impact the crystallization process.[38] CNCs with higher crystallinity and Cin-CNCs with more branch chains and lower crystallinity can have different

Table 2 DSC profile of PLA/CNC films and PLA/Cin-CNC films at different contents

Sample	T_g (°C)	T_{cc} (°C)	T_{m1} (°C)	T_{m2} (°C)
PLA	58.3	116.7	149.4	—
PLA/CNC-0.5%	58.1	109.7	146.5	154.0
PLA/CNC-1%	58.2	113.7	147.5	153.0
PLA/CNC-3%	58.2	111.9	146.4	152.7
PLA/CNC-5%	56.4	103.9	141.0	150.8
PLA/Cin-CNC-0.5%	57.8	111.8	146.8	153.7
PLA/Cin-CNC-1%	55.4	107.2	143.2	152.4
PLA/Cin-CNC-3%	55.2	108.1	140.8	150.5
PLA/Cin-CNC-5%	54.8	107.4	138.6	148.8

impacts on the thermal behavior of PLA. Cin-CNCs had a greater effect on the crystallization transition of PLA due to the enhanced chain mobility. After adding Cin-CNCs, the double melting peaks became more pronounced and T_m shifted to a lower temperature. Hence, notably, the addition of CNCs or Cin-CNCs led to an imperfect crystal structure in PLA.

3.2.3 Mechanical properties. Tensile testing was carried out to investigate the mechanical properties of the PLA and PLA nanocomposite films, as shown in Fig. 8. The addition of CNCs initially improved the tensile strength and the Young's modulus of the PLA films, as shown in Fig. 8a and b, respectively. However, as the filler content increased, the performance began to deteriorate due to particle agglomeration. The maximum tensile strength and Young's modulus values were at 1 wt% CNC addition and they increased by 56% and 30%, respectively, compared to neat PLA film. On the other hand, the addition of Cin-CNCs improved the tensile strength and Young's modulus up to 70% and 37%, respectively, at 3 wt% Cin-CNCs. At a higher filler content, the performance decreased. This enhancement of tensile properties was attributable to the effect of cellulose nanocrystals on reinforcement. When CNCs are added to PLA, they create a network of fibers within the polymer matrix, thereby increasing its tensile strength. The high aspect ratio of nanocellulose increased the surface area for stress transfer between the fillers and polymer matrix, which improved the load-bearing capacity of the composite material.[14] Notably, the optimal number of fillers added to PLA for the best tensile properties varies depending on the degree of nanoparticle dispersion. Due to their hydrophilic surface, excessive CNCs can cause aggregation and create weak points in composite materials, resulting in diminished tensile strength. Consequently, Cin-CNCs clearly demonstrated a significant increase in tensile strength and Young's modulus of PLA due to their hydrophobic, compatible, and well-dispersed nature in the PLA matrix. These cinnamate-functionalized CNCs affected the tensile strength and Young's modulus of the PLA by strengthening the interparticle bond between the filler and the matrix. Due to increased stiffness and decreased flexibility, the resulting material could have a higher tensile strength and Young's modulus.

As shown in Fig. 8c, the addition of CNCs or Cin-CNCs to the PLA matrix substantially reduced elongation at break. The reduction was clearly visible with CNC addition, even at a low

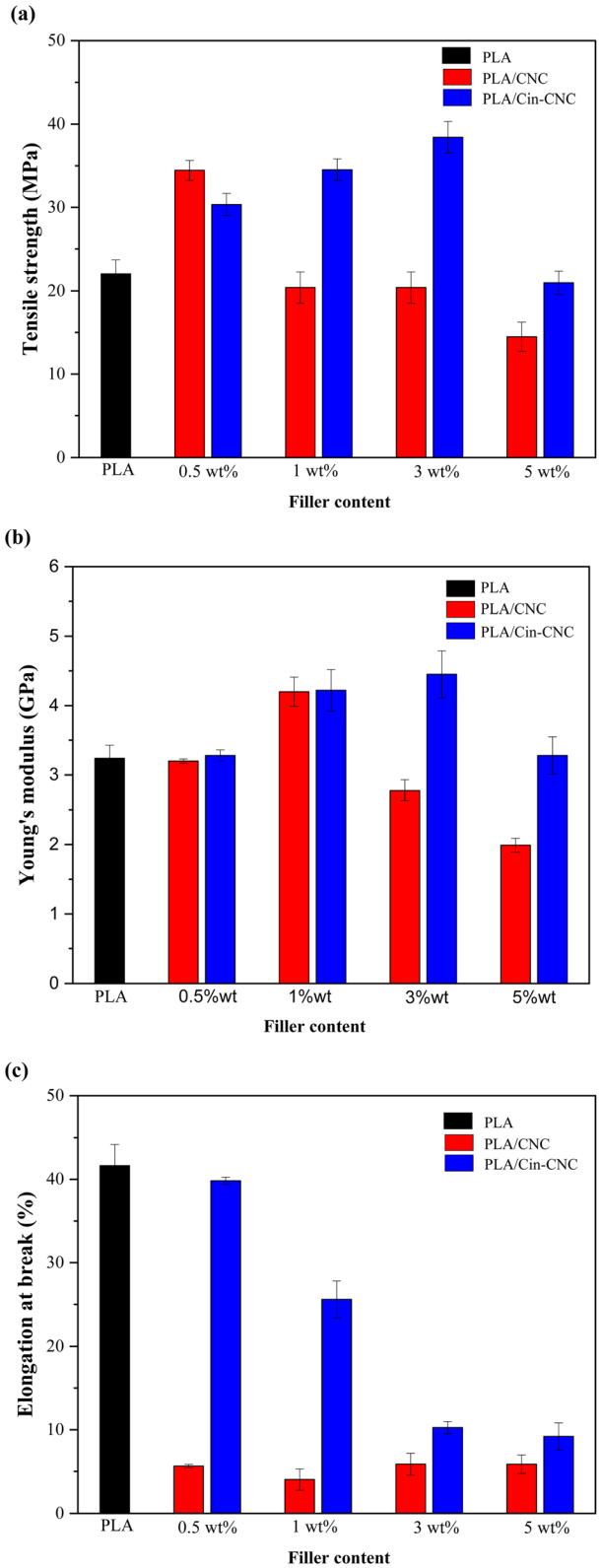

Fig. 8 Mechanical properties of PLA, PLA/CNC, and PLA/Cin-CNC films (a) tensile strength, (b) Young's modulus, and (c) elongation at break. The standard deviation of at least five measurements is denoted by the Y-error bars.

filler content. In contrast, for Cin-CNC addition, the elongation at break was slightly diminished at low concentrations and more pronounced at high concentrations. The elongation at break of a polymer is a measure of its ductility, or ability to stretch and deform before breaking. As observed in DSC thermograms, the addition of CNCs or Cin-CNCs reduces the crystallinity of the polymer chains, making it more difficult for the chains to slide past each other during deformation.[14] As the material becomes more brittle and prone to cracking or fracturing, these results may contribute to a decrease in elongation at break. Furthermore, at higher concentrations where the CNC nanoparticles are poorly dispersed within the polymer matrix, they can act as stress concentrators, initiating cracks or fractures in the material.[4] The crystallinity of CNCs can lead to a reduction in the elongation at break,[14] as the material becomes more prone to failure at lower levels of deformation. As a result, in the current study, the PLA with Cin-CNCs had higher elongation at break than the PLA with CNCs due to the branching chains of the cinnamate group being loosely tangled, resulting in a decrease in crystallinity.[3]

3.2.4 UV radiation absorption. The UV absorption properties of the PLA nanocomposite films were investigated using UV-Vis spectroscopy. As shown in Fig. 9, the pure PLA film had zero UV absorption, indicating high transmittance in the visible range. In addition, adding CNCs into the PLA matrix had a negative impact on UV absorption by the PLA films. In contrast, with the PLA/Cin-CNC films, there was substantial enhancement of UV absorption in the wavelength range 280–320 nm (the UVB region). This strong UV absorption increased directly with increasing Cin-CNC content, suggesting good miscibility between the Cin-CNCs and the PLA. The mechanism by which cinnamate absorbs UV radiation involves electronic transitions within the molecule, as shown in Fig. 10. Due to the conjugated double bonds in cinnamate, the molecule absorbs a photon of UV light *via* π–π* electronic transitions.[17] As

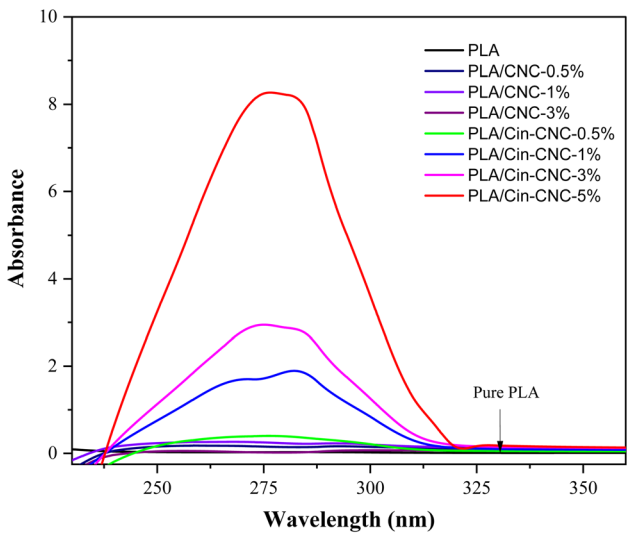

Fig. 9 UV radiation absorption of PLA, PLA/CNC, and PLA/Cin-CNC films.

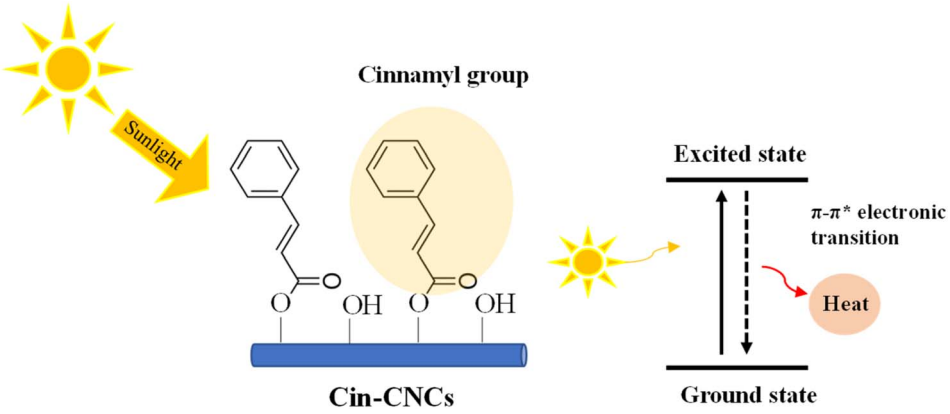

Fig. 10 Schematic mechanism for Cin-CNCs as UV absorbers.

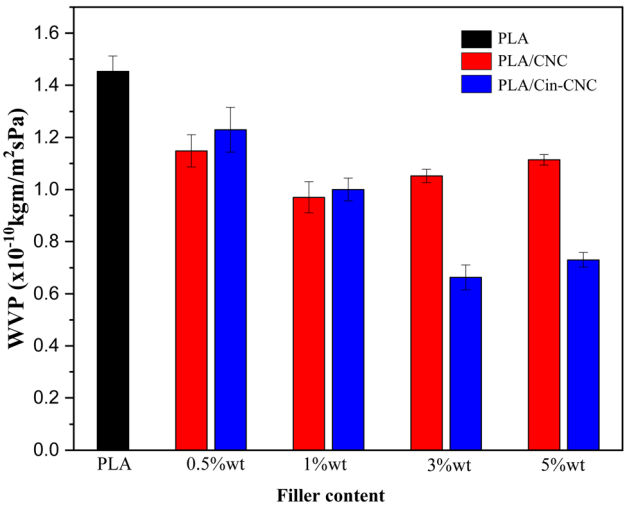

Fig. 11 Water vapor permeability (WVP) of PLA, PLA/CNC, and PLA/Cin-CNC films. The standard deviation of at least three measurements is denoted by the Y-error bars.

a result, an electron is promoted from its highest occupied molecular orbital (HOMO) to its lowest unoccupied molecular orbital (LUMO).[16] The absorption of UV light causes the cinnamate molecule to transition from its ground state to an excited state. This excited state is unstable and rapidly returns to the ground state, releasing excess energy as heat. Hence, the Cin-CNC particles acted as a UV-absorbing agent in the PLA film, effectively shielding the underlying polymer from damage.

3.2.5 Water vapor permeability (WVP) and oxygen permeability (OP). The WVP and OP for the pure PLA and PLA nanocomposite films are shown in Fig. 11 and 12, respectively. The WVP and OP values of the PLA were greatly reduced when CNCs or Cin-CNCs were added in any of the formulations. The addition of CNCs decreased the WVP and OP values of PLA by approximately 33% and 60%, respectively, at 1 wt%. However, at higher concentrations, the WVP and OP slightly increased, which could have been due to the agglomeration of CNCs. The permeability improvement was somewhat less effective at 1 wt% filler content when Cin-CNC was added, with the WVP and OP values being reduced by 31% and 53%, respectively. However, as the Cin-CNCs concentration increased, the WVP and OP of the PLA continued to decrease. The greatest reductions in the WVP and OP values of the PLA were 54% and 55%, respectively, at 3 wt% Cin-CNCs.

CNCs have been extensively investigated as effective gas barriers in polymer matrices, with similar findings reported in the literature to the present study.[27] CNCs can improve the barrier properties by slowing down the diffusion of gas molecules through the polymer matrix. The formation of hydrogen bonds between the hydroxyl groups on the CNCs and the PLA matrix is one possible mechanism.[4] This mechanism creates a strong interfacial adhesion between the two materials, reducing the amount of free volume available for water molecules to diffuse through, thus effectively lowering the material's WVP and OP.[14]

However, this mechanism depends on several factors, including the concentration, dispersion, and surface chemistry of nanocellulose. At high concentration, CNCs tend to generate

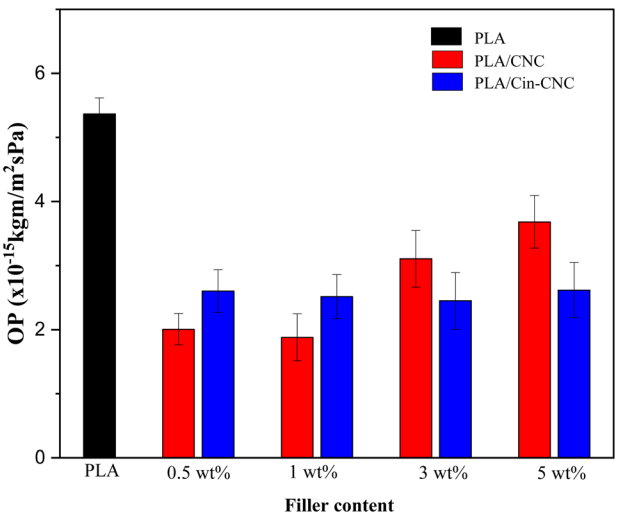

Fig. 12 Oxygen permeability (OP) of PLA, PLA/CNC, and PLA/Cin-CNC films. The standard deviation of at least three measurements is denoted by the Y-error bars.

agglomerations, which negatively affect the gas permeability. In the present work, CNCs were a better barrier than Cin-CNCs at a low filler content in which such agglomerations were not present. Conversely, at higher concentration, Cin-CNCs were a more effective barrier due to the lower WVP and OP of the PLA. These results were caused by functionalization of the cinnamate group on the CNC surface, which generated strong bonding at the filler-polymer interphase, creating a tortuous diffusion path for water and oxygen molecules. A network of strong interparticle interactions within the PLA matrix can create a maze-like structure that gas molecules must navigate to move through the material. This can effectively increase the diffusion path length and reduce the WVP and OP of the material.

4. Conclusions

A UV-shielding material based on cellulose nanocrystals was developed and applied as a nano-reinforcement in PLA film. Acid hydrolysis was used to extract CNCs from pineapple leaves, which were then modified using cinnamoyl chloride through esterification reactions. The Cin-CNCs had a rod-like structure with a 7 nm average diameter and 98 nm average length. FTIR and TGA confirmed the grafting of the cinnamate group to the CNC surface. Thermal properties revealed that the addition of Cin-CNC reduced T_g and T_m slightly. Importantly, grafting the cinnamate group onto CNCs improved their dispersion in PLA matrices and increased substantially the reinforcing effect of the Cin-CNCs. The Cin-CNC addition increased the PLA tensile strength and Young's modulus up to 70% and 37%, respectively. The PLA films with the Cin-CNC addition provided excellent UV absorption; higher filler concentrations provided more UV absorption, without affecting the mechanical properties of the film. The addition of Cin-CNCs also reduced the WVP and OP of the PLA films. Optimizing the concentration and dispersion of Cin-CNCs within the PLA matrix improved the material's barrier properties against oxygen permeation. The greatest reductions in the WVP and OP of the PLA/Cin-CNC films were 54% and 55%, respectively, compared to neat PLA, making these films more useful and versatile for a variety of applications.

Author contributions

Kanokporn Pornbencha: methodology, validation, formal analysis, and writing original draft. Sarannuch Sringam: methodology and formal analysis. Supicha Piyanirund: methodology and formal analysis. Anusorn Seubsai: resources and supervision. Paweena Prapainainar: resources and supervision. Chalida Niumnuy: resources and supervision. Supacharee Roddecha: resources and supervision. Peerapan Dittanet: conceptualization, formal analysis, validation, supervision, project administration investigation, writing-reviewing & editing.

Conflicts of interest

There are no conflicts to declare.

Acknowledgements

The authors would like to thank the Faculty of Engineering, Kasetsart University, the Center of Excellence on Petrochemical and Materials Technology (PETROMAT), the Fundamental Fund, Thailand: FF(KU)12.66, and the Kasetsart University Research Development Institute (KURDI), Bangkok, Thailand for financial support.

References

1 L. T. Sin, A. R. Rahmat and W. A. W. A. Rahman, *Polylactic Acid*, 2013, pp. 1–70.
2 C. Sun, S. Wei, H. Tan, Y. Huang and Y. Zhang, *J. Chem. Eng.*, 2022, **446**, 136881.
3 J. Lu, C. Sun, K. Yang, K. Wang, Y. Jiang, R. Tusiime, Y. Yang, F. Fan, Z. Sun, Y. Liu, H. Zhang, K. Han and M. Yu, *Polymers*, 2019, **11**(6), 1009.
4 M. Szymańska-Chargot, M. Chylińska, P. M. Pieczywek, A. Walkiewicz, G. Pertile, M. Frąc, K. J. Cieślak and A. Zdunek, *Polymers*, 2020, **12**(4), 812.
5 D. DemirgoÈ, C. Elvira, J. F. Mano, A. M. Cunha, E. Piskin and R. L. Reis, *Polym. Degrad. Stab.*, 2000, **70**, 161–170.
6 L. Cao, C. Liu, D. Zou, S. Zhang and Y. Chen, *Carbohydr. Polym.*, 2020, **230**, 115618.
7 Y. Liu, S. Ahmed, D. E. Sameen, Y. Wang, R. Lu, J. Dai, S. Li and W. Qin, *Trends Food Sci. Technol.*, 2021, **112**, 532–546.
8 A. K. Rana, E. Frollini and V. K. Thakur, *Int. J. Biol. Macromol.*, 2021, **182**, 1554–1581.
9 K. Pornbencha, T. Boonmalert, A. Seubsai and P. Dittanet, *Key Eng. Mater.*, 2021, **891**, 131–136.
10 S. Sun, S. Sun, X. Cao and R. Sun, *Bioresour. Technol.*, 2016, **199**, 49–58.
11 O. Y. Alothman, L. K. Kian, N. Saba, M. Jawaid and R. Khiari, *Ind. Crops Prod.*, 2021, **159**, 113075.
12 H. Zhang, Y. Chen, S. Wang, L. Ma, Y. Yu, H. Dai and Y. Zhang, *Carbohydr. Polym.*, 2020, **238**, 116180.
13 E. Fortunati, F. Luzi, D. Puglia, R. Petrucci, J. M. Kenny and L. Torre, *Ind. Crops Prod.*, 2015, **67**, 439–447.
14 Z. Wang, Z. Yao, J. Zhou, M. He, Q. Jiang, A. Li, S. Li, M. Liu, S. Luo and D. Zhang, *Int. J. Biol. Macromol.*, 2019, **129**, 878–886.
15 Z. Zhen, Z. Boya, G. Nathan, B. Richard and C. T. Kam, *Adv. Sustainable Syst.*, 2019, **3**(4), 1800156.
16 Z. Zhang, K. C. Tam, X. Wang and G. Sèbe, *ACS Sustainable Chem. Eng.*, 2018, **6**(2), 2583–2590.
17 Z. Wang, X. Zhuang, Y. Chen, B. Wang, J. Yu, W. Huang, T. J. Marks and A. Facchetti, *Chem. Mater.*, 2019, **31**(18), 7608–7617.
18 W. Wu, S. Karamdoust, B. A. Turowec and E. R. Gillies, *Eur. Polym. J.*, 2013, **49**(12), 4238–4248.
19 C. Zhu, S. R. Kustra and C. J. Bettinger, *Acta Biomater.*, 2013, **9**(7), 7362–7370.
20 V. Bugatti, L. Vertuccio, S. Zara, F. Fancello, B. Scanu and G. Gorrasi, *Carbohydr. Polym.*, 2019, **209**, 356–362.
21 P. Dhatarwal and R. J. Sengwa, *Optik*, 2021, **241**, 167215.

22 W. Xie, E. Pakdel, D. Liu, L. Sun and X. Wang, *ACS Sustainable Chem. Eng.*, 2019, **8**(3), 1343–1352.
23 A. Daochalermwong, N. Chanka, K. Songsrirote, P. Dittanet, C. Niamnuy and A. Seubsai, *ACS Omega*, 2020, **5**(10), 5285–5296.
24 L. Ravindran, M. S. Sreekala and S. Thomas, *Int. J. Biol. Macromol.*, 2019, **131**, 858–870.
25 *Standard Test Method for Tensile Properties of Thin Plastic Sheeting*, **https://www.astm.org/d0882-18.html**, accessed April 2023.
26 *Standard Test Method for Water Vapor Transmission Rate of Sheet Materials Using Dynamic Relative Humidity Measurement*, **https://www.astm.org/e0398-03.html**, accessed April 2023.
27 S. S. Karkhanis, N. M. Stark, R. C. Sabo and L. M. Matuana, *Composites, Part A*, 2018, **114**, 204–211.
28 *Standard Test Method for Oxygen Gas Transmission Rate Through Plastic Film and Sheeting Using a Coulometric Sensor*, **https://www.astm.org/d3985-17.html**, accessed April 2023.
29 A. Daochalermwong, N. Chanka, K. Songsrirote, P. Dittanet, C. Niamnuy and A. Seubsai, *ACS Omega*, 2020, **5**, 5285–5296.
30 M. Sasikala and M. J. Umapathy, *New J. Chem.*, 2018, **42**(24), 19979–19986.
31 J. I. Morán, V. A. Alvarez and V. P. Cyras, *Cellulose*, 2007, **15**(1), 149–159.
32 N. Pandi, S. H. Sonawane and K. Anand Kishore, *Ultrason. Sonochem.*, 2021, **70**, 105353.
33 S. Rasha, K. Hanieh and A. Ibrahim, *Sains Malays.*, 2015, **44**(6), 801–810.
34 P. Huang, Y. Zhao, S. Kuga, M. Wu and Y. Huang, *Nanoscale*, 2016, **8**(6), 3753–3759.
35 S. Hua, F. Chen, Z. Liu, W. Yang and M. Yang, *RSC Adv.*, 2016, **6**(3), 1973–1983.
36 Y. Song, K. Tashiro, D. Xu, J. Liu and Y. Bin, *Polymer*, 2013, **54**(13), 3417–3425.
37 C. Miao and W. Y. Hamad, *Carbohydr. Polym.*, 2016, **153**, 549–558.
38 E. Vatansever, D. Arslan, D. S. Sarul, Y. Kahraman and M. Nofar, *Int. J. Biol. Macromol.*, 2020, **154**, 276–290.